Acta Geotechnica (2024) 19:1891–1909
https://doi.org/10.1007/s11440-023-01984-4

RESEARCH PAPER

# Instrumented column testing on long-term consolidation and desiccation behaviour of coal tailings under natural weather conditions

Wenqiang Zhang[1] · Chenming Zhang[1] · Ximing Lei[1] · Sebastian Quintero Olaya[1] · Yuyang Zhu[1] · Zicheng Zhao[1] · Steve Jensen[2] · David John Williams[1]

Received: 14 December 2021 / Accepted: 26 June 2023 / Published online: 3 August 2023


**Abstract**
The sedimentation, consolidation and desiccation behaviour of sub-aerially deposited tailings in tailings storage facilities, despite occurring simultaneously and being essential to maximise tailings dry density and dewatering efficiency, are usually analysed in laboratories using distinctive testing equipment, which is unable to reveal their interactions. A large instrumented column was constructed to test the three processes of tailings in a single apparatus, capable of monitoring the changes in the hydrological parameters of coal tailings with depth and surface settlement under natural weather conditions. The column was initially filled with coal tailings slurry and exposed to natural weather for two years, during which five wetting–drying periods were identified. The monitored results indicate that exposing the slurry tailings for one month would lead to the formation of an unsaturated tailings layer with a thickness of 150 mm, likely representing the optimised tailings deposition cycle and thickness, respectively, under the given tailings characteristics and semi-arid climates. Settlement mainly occurred after major rainfall events due to the collapse of cracks and cavities formed during the preceding desiccation. The maximum thickness of the unsaturated tailings increased over the first four periods as the predominant desiccation and settlement strengthened the evaporative capillary forces, despite it decreasing greatly in the last period due to insufficient desiccation. An empirical model was proposed to consecutively estimate the surface moisture content of deformable tailings and validated by achieving a good agreement in the water mass estimated by two methods during wetting–drying cycles.

**Keywords** Coal tailings · Consolidation · Desiccation · Evaporation · Settlement · Surface moisture content

## 1 Introduction

Coal tailings, a mixture of water and finely sized rock and mineral solids, are the main waste product generated in mine processing and are normally deposited in tailings storage facilities (TSFs) as a wet slurry [4, 26]. Since it averagely accounts for 80% of the total mass of coal waste, economical disposal of tailings with minimising detrimental effects on the environment has become a significant concern for the mining industry [13]. In arid and semi-arid regions, the aforesaid problems are effectively mitigated using sub-aerial deposition, by which tailings mainly undergo sedimentation, consolidation and desiccation [29, 41]. Developing a comprehensive understanding of the above physical processes and the corresponding behaviours of soft tailings is crucial for effective waste management and efficient operations of TSFs [5, 33].

Rather than natural soils, tailings behave non-uniformly in their engineering parameters due to the diverse nature of raw ore and handling methods [1, 4]. By conducting a series of laboratory tests, Qiu and Sego [28] investigated the basic physical and engineering parameters of four typical mine tailings and concluded that coal wash tailings exhibited clayey silt characteristics with plastic cohesive

✉ Chenming Zhang
chenming.zhang@uq.edu.au

[1] School of Civil Engineering, The University of Queensland, Brisbane, QLD 4072, Australia

[2] Meandu Mine–Tarong Power Station, Stanwell Corporation Limited, Kingaroy, QLD 4601, Australia

behaviour, which entirely differed from copper, gold and oil sand tailings. Silty coal tailings are often transported to TSFs as slurries with high water content and then deposited for further static dewatering [4]. The deposited tailings slurry first goes through sedimentation, during which the suspended solid particles settle due to gravity without the development of effective stress, and tailings surface elevation decreases.

Sedimentation completes in a few days, with supernatant water ponded above the surface tailings. Subsequent self-weight consolidation lasts much longer due to the gradual increment of effective stresses and dissipation of pore water pressures within the solid skeleton, which results in significant surface settlement [20, 32]. The consolidation behaviour of tailings slurry can be an essential aspect influencing the stability of tailings dams and the operation of tailings disposal [33, 47]. Through the previous research, large amounts of laboratory tests have been conducted to determine consolidation properties of tailings using different methods, such as constant rate of deformation (CRD) tests [5, 8, 31, 46], oedometer tests [19, 33], Rowe cell tests [25], slurry consolidometer tests [6, 42] and column tests [28, 35]. The individual and combined effects of mineralogy, compressibility, hydraulic conductivity, void ratios and shear strength on consolidation behaviours of soft tailings were examined in past studies [1, 21]. However, conventional consolidation tests are generally carried out by using specimens in saturated states, which means no gaseous phase flow is considered during the whole procedure.

In addition to sedimentation and consolidation, desiccation is a key process that sub-aerially deposited tailings experience in TSFs. Different from consolidation, desiccation is driven by evaporation on the tailings surface, during which consolidated particles are further compressed with water expelled from pore spaces due to the building up of capillary pressure. This process accelerates the densification of tailings and hence is advantageous for enhancing the stability and rehabilitation of TSFs [16, 37]. Recent research has been focusing on characterising the desiccation behaviour of tailings and exploring its interactions with consolidation. For example, Rodríquez et al. [30] found that tailings porosity greatly affects its water-holding capacity and saturated hydraulic conductivity, and the permeability and mechanical properties of the tailings strongly rely on the evolution of the degree of saturation during the desiccation process. Based on the vertical hydraulic gradient between the fresh layer and the desiccated gold tailings in a modular drying box, Daliri et al. [11] divided the desiccation behaviour of multi-layer gold tailings into two phases: high average water content with rapid drainage and settling (phase I) and low average water content ($< 30\%$) with slow evaporation rate (phase II). The desiccation of fresh tailings in phase I was accelerated due to the predominant downward water movement and the strengthened capillary forces of the underlying tailings, while the desiccation was decelerated in phase II due to the slow upward water recharge from the underlying tailings. Furthermore, to be consistent with field conditions, Shokouhi et al. [36] used a large-scale slurry consolidometer to successfully implement the settling, consolidation and evaporation processes. They pointed out that the majority (88%) of settlement occurred during the settling process, and the consolidated coal tailings slurry tended to desiccate faster than the non-consolidated ones due to enhanced capillary forces and hydraulic conductivity. To quantify the desiccation rate in soil or soil-like material, Zhang [43] analysed the influencing factors of soil evaporation and highlighted the importance of moisture content on the surface, which determines water transfer through the soil-air interface [44]. Determination of soil surface moisture contributes to obtaining surface resistance and quantifying the actual evaporation rate. In an attempt to build a relationship between surface resistance and liquid water saturation at the soil surface, large numbers of studies have developed various forms of surface resistance models (e.g. the linear equation given by Camillo and Gurney [7] and Meng et al. [23], the exponential function proposed by Van de Griend and Owe [39] and the power-law put forward by Daamen and Simmonds [10]) to better quantify the desiccation rate of soil or soil-like materials.

Although taking place simultaneously, the three processes (sedimentation, consolidation and desiccation) usually need to be tested separately for characterisation and use individual tailings samples under conventional lab testing methods in idealised environments, which may lead the testing results not to be representative of field conditions. Therefore, there is a need to develop one experimental apparatus to achieve testing the three processes and simulate sub-aerial deposition in TSFs. To gain a clearer understanding of the long-term self-weight consolidation and desiccation behaviour of tailings under natural weather conditions and quantitatively evaluate settlement and evaporation processes in repeated wetting–drying periods, a large instrumented column was constructed on a building roof and filled with a coal tailings slurry. The tailings slurry was exposed to natural weather, along with a weather station to monitor the ambient meteorological conditions. When calculating the actual evaporation rates of the tailings, an empirical model was developed to extrapolate the degree of saturation at the tailings surface as settlement progresses, capable of adjusting the surface resistance for further quantifying the water mass balance in the column. The model was verified by achieving good agreement between the water storages estimated from rainfall and evaporation data and from the moisture sensor

array measurements. This paper documents in detail the establishment of the column and presents two-year results obtained from the test to characterise the consolidating and dewatering behaviour of coal tailings in response to natural meteorological changes.

## 2 Experimental method

### 2.1 Instrumented column design

The integrated sedimentation, consolidation and desiccation test of the coal tailings under natural weather conditions was conducted using an instrumented column. As depicted in Fig. 1, the cylindrical column was designed with a height of 1.2 m, much more than the depth of the unsaturated zone formed during desiccation, ensuring the result is independent of the column height. The diameter of the column is 200 mm, at which the wall effect can be minimised [36, 45]. The bottom of the column was sealed, and the top of the column was open to the sun and atmosphere. The column consisted of two sections, each with a height of 0.6 m, connected by a waterproof flange. This facilitated the sensor installation and removal, before and after the experiment. Ten dielectric moisture sensors and ten thermal sensors developed by the Geotechnical Engineering Centre (GEC) at The University of Queensland (UQ) were used to measure volumetric water content (VWC) and tailings temperature indirectly. The in-house developed moisture sensor is designed to measure the VWC of tailings via its changes in dielectric permittivity.

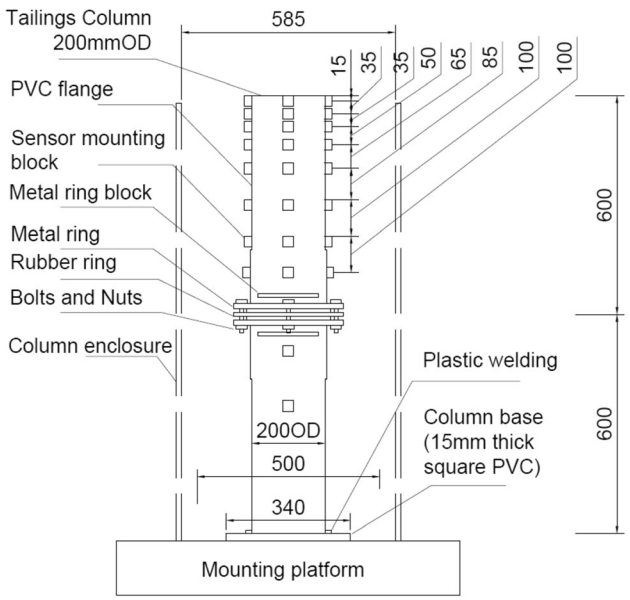


**Fig. 1** Schematic diagram of the instrumented column (all dimensions in millimetres)

Such a moisture sensor could provide reliable and continuous measurements with relatively low disturbance by the increasing salinity level in the soil. The thermal conductivity sensor consists of a thermocouple and a porous ceramic cylinder, capable of measuring tailings temperatures with variations in water contents. The sensors were installed through the column wall at incremental depth intervals downwards from the surface to the bottom (i.e. 15, 50, 80, 135, 200, 285, 385, 485, 700, 850 mm from the opening surface of the column), and each set of sensors was fixed at quarter points around the perimeter of the column. Two DECAGON GS3$^{TM}$ moisture sensors were buried at 50 mm and 600 mm depths to measure the bulk salinity of the tailings indirectly via electrical conductivity (EC).

In addition to the sensors mentioned above, the surface settlement and cracking were captured by a high-resolution camera mounted above the column facing the tailings surface. All instruments were connected to a solar-powered data logger, also developed by GEC at UQ, capable of transmitting monitored data simultaneously to a website for visualisation and analysis.

### 2.2 Experimental procedure

#### 2.2.1 Material characterisation and preparation

The coal tailings were obtained from the Meandu Mine, from where tailings were transported to a TSF near Tarong Power Stations of Stanwell Corporation Limited, located in the South Burnett region of Queensland, Australia. The particle size distribution curve (Fig. 2a) was obtained through wet sieving and hydrometer analysis (for particle size less than 75 μm), revealing that the fine particles (size less than 75 μm) are dominant for the studied coal tailings. The measured soil–water characteristic curve (SWCC) of the coal tailings is presented in Fig. 2b, fitted with the van Genuchten model. The air entry value (AEV) of the tailings sample is around − 3 kPa, reflecting relatively large pore spaces between solid particles. Such a low AEV of the fine-fraction-dominated tailings is probably due to the high content of coal and its effect of hydrophobicity [40]. Note that the tailings sample was compacted before putting into the SWCC apparatus, mainly to avoid significant density change during the test. Table 1 presents the main geotechnical parameters of the coal tailings. The specific gravity of the specimen was the same as the value reported by Qiu and Sego [28], and the Atterberg limits of the coal tailings were close to the range given by Islam et al. [20]. The tailings can be classified as silty clay (based on the Unified Soil Classification System) of high plasticity. The selected coal tailings samples were first put into an oven for drying with temperature restricted to 60 °C to avoid combustion of any coal content. The oven-dried tailings were

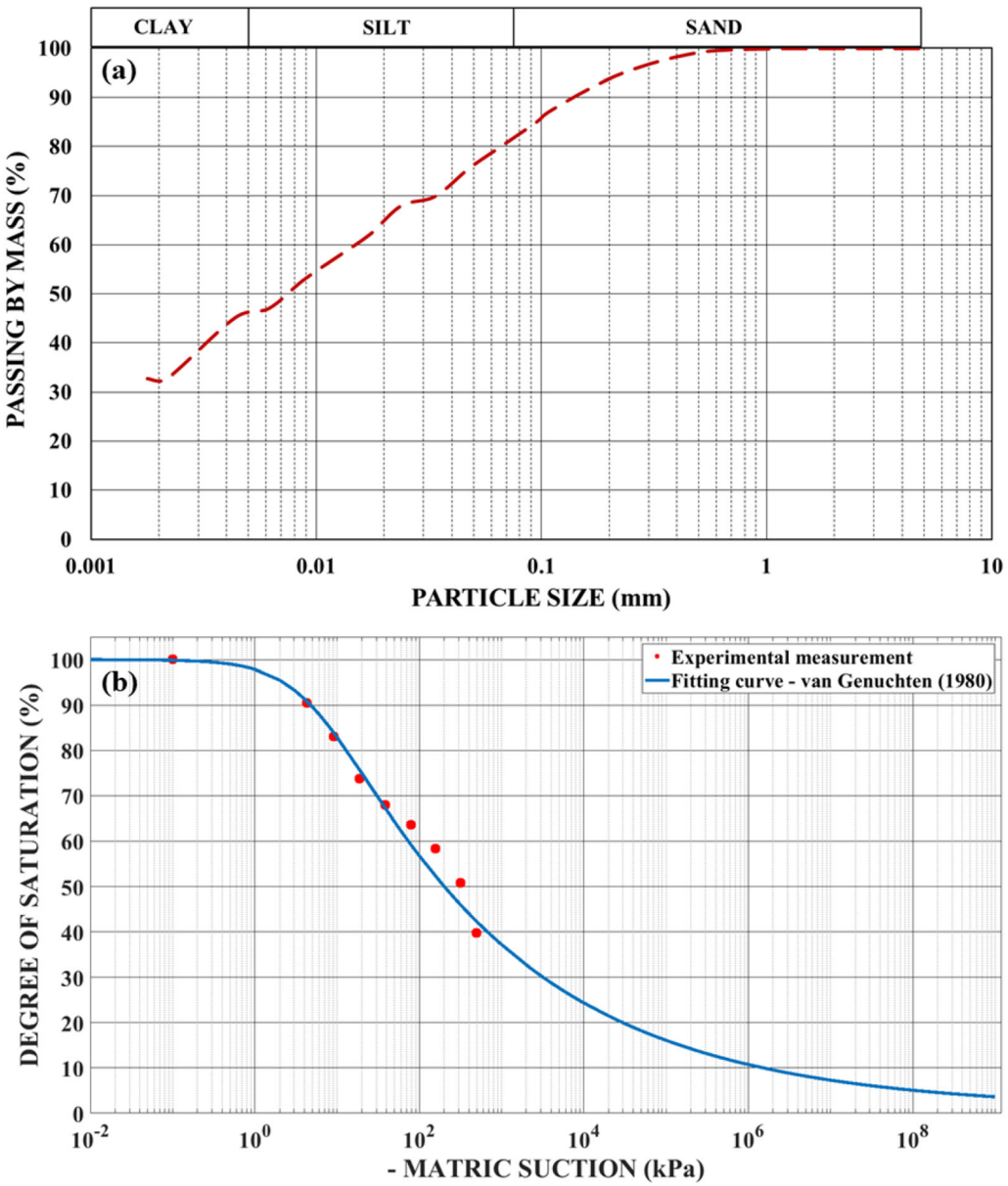


**Fig. 2** Characterisation of the coal tailings: **a** particle size distribution curve; **b** lab-measured soil–water characteristic curve (SWCC) of the compacted coal tailings, fitted with van Genuchten (VG) 1980 model

pulverised into powders using a rubber pestle, and coal processing water was added to achieve 40% solids concentration by mass.

### 2.2.2 Sensor calibration

Prior to the column construction, all sensors were calibrated in the laboratory by inserting them into the same coal tailings (void ratio of 2.92 and dry density of 0.497 t/m$^3$) subjected to repeated wetting and drying cycles. The thickness of the tailings was about 40 mm to avoid uneven distribution of moisture with depth. The basin containing both the tailings and sensors was placed on an electrical balance to record the weight changes resulting from water gain or loss, which could be correlated to the VWC of the tailings. During the wetting and drying cycles, both the weight changes and sensor readings were recorded. The calibration was done by correlating the VWC derived from the weight of the tailings and that measured by the sensors. Figure 3 shows the calibration chart of the moisture sensor. A non-linear relationship between degree of saturation and sensor response was fitted with the average results between two wetting–drying curves to interpret the data obtained in the column test. This fitting curve is capable of interpreting moisture changes in the tailings during wetting–drying cycles and accommodating deviations in moisture

**Table 1** Hydrological and geotechnical parameters of the coal tailings

| Parameters | Value |
|---|---|
| Specific gravity | 1.949 |
| Dry density (kg/m$^3$) | 497 |
| Solids content (%) | 40 |
| Liquid limit (%) | 48.1 |
| Plastic limit (%) | 24.3 |
| Plasticity index (%) | 23.8 |
| Clay-sized particles (%) | 32.8 |
| Silt-sized particles (%) | 52.3 |
| Sand-sized particles (%) | 14.9 |
| Air entry value (kPa) | − 3 |
| Saturated hydraulic conductivity (m/s) | $4.08 \times 10^{-7}$ |

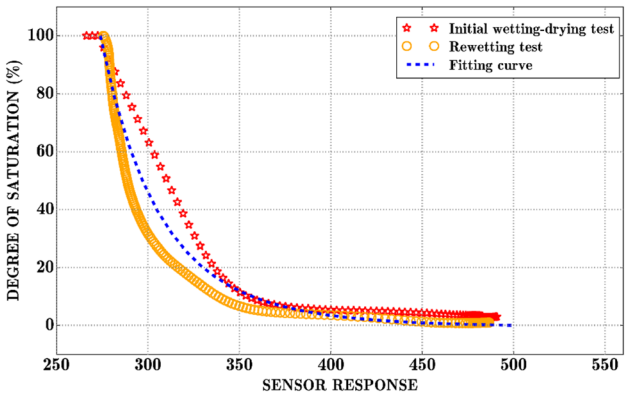


**Fig. 3** Calibration chart of the in-house moisture sensor

measurement due to settlement. It is worth mentioning that this calibration assumes the dielectric permittivities of the tailings are mainly affected by the changes in the moisture content. Although factors such as density, temperature and salinity of the tailings can also affect the dielectric permittivity of the bulk tailings, their effects are relatively less significant, particularly when the tailings experience from full water saturation to an air-dry condition [18, 38]. The thermal sensor provided direct Celsius temperature as output and was calibrated against readings from a hand-held thermometer. The difference between the two measurements was found to be negligible, indicating the in-house thermal sensor is reliable in capturing temperature variations in the sample during the monitoring test.

#### 2.2.3 Column setup and test procedure

After calibration, the sensors were mounted through cable glands on the column wall (Fig. 4a). An extra column section with a height of 100 mm was temporarily installed above the column with the joints sealed to accommodate supernatant water during the slurry tailings deposition. Moreover, a waterproof test was done by filling the column with tap water and covering it with a plastic film over two weeks to ensure that the water level did not drop due to leaking.

After the waterproof test, the instrumented column was positioned on the roof of a building, where a weather station was deployed nearby. The coal tailings slurry was then carefully poured into the column in a series of layers. Each layer of the slurry was about 200 mm thick, and the solids would settle to a depth of 100 mm, leaving clear supernatant water on top. Following the settling, which is normally completed in one day, the supernatant water was removed before the next layer of slurry tailings was added. Such a process was repeated until the settled tailings solids reached a height of 1.2 m. The temporarily-installed top column section was then removed, allowing the tailings surface to be freely exposed to sunlight and wind. The column was enclosed by four polyvinyl chloride (PVC) panels to prevent it from being tipped over by strong winds and to minimise the direct sunlight exposure to the side of the column (Fig. 4c). Temperature, moisture content and EC of the tailings in the column were measured by the sensors on an hourly basis, and the weather conditions were recorded every eight minutes. Images on the tailings surface were taken three times per day (i.e. 9 am, 12 pm, 3 pm) to document settlements, ponding and cracking.

After several wetting–drying cycles, the surface of tailings settled below the column top, impeding wind and sun exposure when the surface was dry and causing the formation of a pond when the surface was wet. Therefore, the top section of the column and associated sensors were removed (Fig. 4e and f) to minimise the boundary impact of the extruding wall.

## 3 Theoretical background

The water mass balance of the tailings in the column under weather can be described as [17]:

$$\frac{\mathrm{d}Q_{\mathrm{w}}}{\mathrm{d}t} = P - \mathrm{ET_A} \tag{1}$$

where $P$ (mm/day) is the rainfall; $\mathrm{ET_A}$ (mm/day) is the actual evaporation; $Q_{\mathrm{w}}$ (mm) is water storage in the column, and $t$ (day) is time.

When pore water on the evaporating surface is fresh and high in saturation, the evaporation rate is determined by the weather factors such as solar radiation intensity, relative humidity, wind velocity and temperature [22, 27]. These factors determine the maximum possible evaporation rate under the given weather condition, which is termed as potential evaporation rate (PER). The actual evaporation


**Fig. 4** Images of the instrumented column assembly processes: **a** top view of sensors layout before deposition of tailings; **b** assembled column with sensors installed; **c** rear view of the column (enclosed by four PVC panels), solar panel and electrical enclosure; **d** top view of the column after the additional top section being removed; **e** front view of the column after the top 150 mm section being trimmed in March 2019; **f** rear view of the trimmed column

rate (AER) from soils may be lower than the PER as the evaporating surface may have insufficient water to be evaporated [12] or the surface becomes hypersaline [15, 45]. Considering the energy balance and water availability on the evaporating surface, the Penman–Monteith equation is widely used in predicting AER [24]:

$$\mathrm{ET_A} = \frac{1}{\lambda}\frac{\Delta(R_\mathrm{n} - G) + \rho_\mathrm{a} c_\mathrm{a}\dfrac{\left(v_\mathrm{a}^* - v_\mathrm{a}\right)}{r_\mathrm{a}}}{\Delta + \gamma\left(1 + \dfrac{r_\mathrm{s}}{r_\mathrm{a}}\right)} \tag{2}$$

where $\lambda$ is the latent heat of vaporisation (MJ/kg) ($\lambda = 2500250 - 2365(T_\mathrm{air} - 273.15)$, with $T_\mathrm{air}$ being air temperature (K) at the reference point above the soil surface) [2]; $R_\mathrm{n}$ is the net solar radiation (W/m); $G$ is the heat flux density of the soil (W/m$^2$); $\rho_\mathrm{a}$ is the mean air density ($\rho_\mathrm{a}$ = 1.27 kg/m$^3$); $c_\mathrm{a}$ is the specific heat capacity of the dry air ($c_\mathrm{a}$ = 1013 J/(kg K)); $v_a^*$ is the saturated vapour pressure (Pa) on the soil surface (

$$v_\mathrm{a}^* = 610\exp(17.27(T_\mathrm{soil} - 273.15)/(T_\mathrm{soil} - 35.85)$$

, with $T_\mathrm{soil}$ being air temperature on the soil surface (K)); $v_\mathrm{a}$ is the actual vapour pressure (Pa) in the air ($v_\mathrm{a} = h_\mathrm{r} v_\mathrm{a}^*$, with $h_r$ being relative humidity (−) at the reference point above the soil surface); $\Delta$ is the derivative of saturated water vapour pressure (Pa/K) with respect to air temperature $T_\mathrm{air}$ (K) ($\Delta = 4098 * v_\mathrm{a}/(T_\mathrm{air} - 35.85)$); $\gamma$ is the psychrometric constant ($\gamma$ = 62.2 Pa/K); $r_a$ is the aerodynamic resistance (s/m) to water vapour transfer ($r_\mathrm{a} = (\ln(2/0.000001))^2/k^2 u_2$, with $k$ = 0.41 being von Karman's constant (-) and $u_2$ being the wind speed (m/s) at 2 m above the soil surface); $r_\mathrm{s}$ is the soil surface resistance (s/m) to water vapour transfer.

An exponential equation proposed by Van de Griend and Owe [39] was used to calculate surface resistance:

$$r_\mathrm{s} = 10e^{35.63\mathcal{E}(S_\mathrm{rmin} - S_\mathrm{rTS})} \tag{3}$$

where $S_\mathrm{rmin}$ is the minimum liquid water saturation (−) below which the liquid water can-not sustain potential evaporation; $e$ is natural logarithm; $S_\mathrm{rTS}$ is the liquid water saturation (−) at the tailings surface; $\mathcal{E}$ is the porosity of

tailings (−). When the evaporating surface is water-saturated, the evaporation rate computed by Eq. (2) equals PER.

It is noted that $S_{rTS}$ in Eq. (3), a key parameter to obtain AER, is acquired from the top soil layer with a thickness of 10 mm. However, obtaining the moisture content at such a thin layer is challenging, particularly when the tailings surface settles and undergoes cracking during desiccation (Fig. 5). As the tailings sample used in this study has a high percentage of silty-sized particles, settlement could be significant during consolidation and desiccation, leading the tailings surface to recede below the top most sensor that is supposed to capture the moisture content near the surface (e.g. Sensor 1 in Fig. 5). Consequently, measurement of the surface moisture conditions and further estimation of AER would be inaccurate. Although within the vertical sensor array, the moisture sensor immediately below the previously air-exposed sensor may be situated in the best location to provide the moisture content at the tailings surface, the distance between that sensor to the surface ($D$ in Fig. 5) could be too far to reveal the surface condition accurately. Such distance may decrease as settlement continues (e.g. Sensor 1 in Fig. 5). Hence, a relationship between $S_{rTS}$ and the degree of saturation measured from the sensor (Sensor 2, Fig. 5) installed underneath ($S_r$) should be explored so that the AER can be estimated from a subsiding tailings surface. With the assumption that the surface settles uniformly during consolidation and enlightened by the soil–water characteristic curve equation proposed by Fredlund and Xing [14], an empirical model to extrapolate $S_{rTS}$, when a pond is absent above the tailings surface, by using the moisture data from the sensor below the surface with a depth of $D$ (m), is suggested:

$$S_{rTS} = S_r\left\{\ln\left[e + \left(\frac{D}{a}\right)^n\right]\right\}^{-m} \tag{4}$$

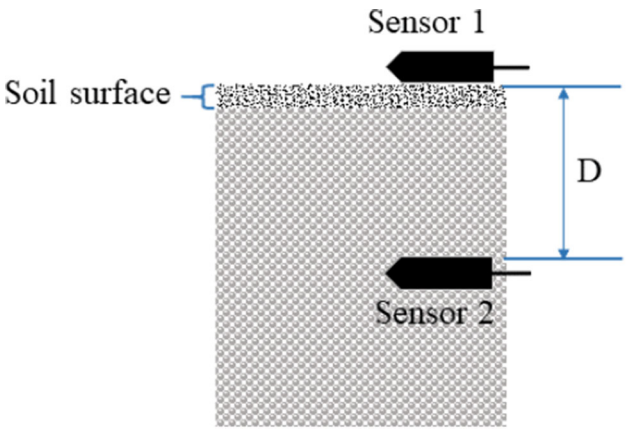


**Fig. 5** Schematic of the soil surface and vertical moisture sensor array after the topmost sensor (sensor 1) is exposed to the air as the surface subsides

where $a$, $n$, $m$ are fitting parameters (−). Equation (4) allows the use of moisture conditions with a significant distance to the surface to extrapolate the surface moisture content and enables the estimation of AER from subsiding tailings. The three parameters $a$, $n$, $m$ in Eq. (4) govern the correlations between $S_r$, $D$ and $S_{rTS}$ and can be determined by comparing (i) the cumulative water mass exchange between the tailings surface (evaporation) and the atmosphere (rainfall), and (ii) the water storage in the tailings estimated by the moisture sensor array, as described by Eq. (1).

Assuming that the dry density of the tailings varies uniformly with depth, the porosity of the tailings is calculated as follows:

$$\varepsilon = 1 - \frac{\rho_d}{G_s} \tag{5}$$

where $\rho_d$ is the dry density (kg/m$^3$) of tailings which varies with settlement ($\rho_d = \rho_{d0}(H_0/H_a)$, where $\rho_{d0}$ (497 kg/m$^3$) being the initial dry density of tailings, $H_0$ being the initial height of the tailings (1.2 m) and $H_a$ being the actual height (m) of the consolidated tailings); $G_s$ is the specific gravity (−).

Considering the height of ponding water above the surface and assuming the degree of saturation in the tailings between two neighbouring sensors can be represented by the mean values measured by the two sensors, the mass of liquid water stored in the column can be estimated by:

$$\begin{aligned} Q_w &= \varepsilon S_{rTS}\cdot(d_i - d_s) + \sum_{i=1}^{k}\frac{\mathcal{E}(S_{ri} + S_{ri+1})}{2} \\ &\quad \cdot(d_{i+1} - d_i) + \mathcal{E}S_{rk}\cdot(H_0 - d_k) + Q_p \end{aligned} \tag{6}$$

where $d_s$ is the cumulative surface settlement (mm); $d_i$ ($i$=1 ∼ 9) is the relative height of the installed moisture sensor array with respect to the bottom of the column (mm); $k$ (10) is the number of the moisture sensors installed (−); $S_{ri}$ ($i = 1 \sim k$) is the degree of saturation measured from each moisture sensor ( - ); $Q_p$ is the depth of ponding water (mm).

## 4 Results and discussion

### 4.1 Weather monitoring

Figure 6 shows the weather condition versus elapsed time, including daily accumulated rainfall, solar radiation, wind speed, air temperature, relative humidity and atmospheric pressure at a reference point 2 m above the column bottom. In general, rainfall occurred mostly during wet seasons between October 2018 and April 2019 (Fig. 6a). In the last three quarters of 2018, the total rainfall was only 261.3 mm, followed by an annual value of 435.8 mm in

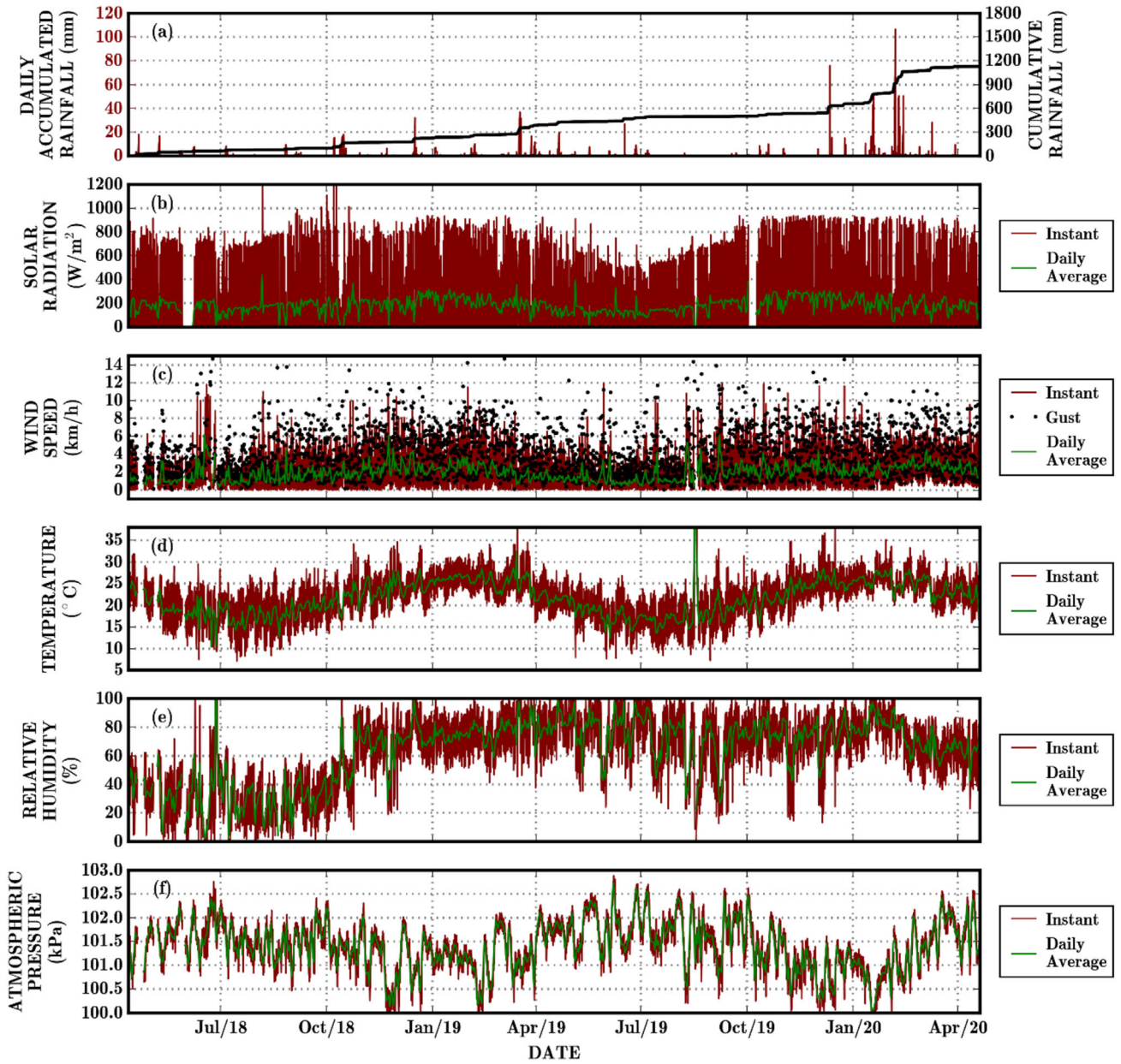


**Fig. 6** Two-year monitored data from the weather station, including **a** daily accumulated rainfall; **b** solar radiation; **c** wind speed; **d** air temperature; **e** relative humidity; **f** atmospheric pressure. Lines in brown represent measured data, and lines in green represent daily averages

2019, which was the driest year based on the last 119-year record from the Australian Bureau of Meteorology (BOM), the cumulative rainfall of the first 111 days in 2020 reached 466 mm, even surpassing the total annual rainfall of 2019. The heaviest rainfall in 2018 was about 31 mm/day, occurring in mid-December, while that in 2019 was about 78 mm/day, occurring in the same month. Also exhibiting an annual sinusoidal pattern, the solar radiation kept steady with daily peak values around $850 \pm 50$ W/m$^2$ in wet seasons (October to April of the next year), whereas fluctuated with peak values between $600 \pm 50$ W/m$^2$ during dry seasons (May to September of the next year). Similarly, the daily wind speed during the wet seasons remained slightly higher (between 6 and 10 km/h) than that in the dry seasons (between 2 and 6 km/h). The air temperature (Fig. 6d) varied consistently with solar radiation. The coldest month of the monitoring period was July 2018 and 2019, with an average temperature of 17 °C, whilst the hottest month was March 2019 with an average value of 27 °C. After declining to the minimum in 2018, relative humidity increased gradually once the wet season arrived and fluctuated at a high value between 60 and 85% for the rest of the monitoring period. Although less rainfall occurred in 2019, relative humidity remained

high throughout that year. In summary, the two-year weather record represents a typical sub-tropical climate, characterised by a transition between El Niño and La Niña periods at the study site.

### 4.2 Tailings parameters monitoring

Figure 7. shows the data measured and derived from the tailings, and the gain (by rainfall) and loss (by evaporation) of water from the tailings surface. In general, PER was high in summer, with an average value of 6 mm/day, and low in winter, with an average value of 3 mm/day (Fig. 7b). Such variation pattern aligns with the changes in solar radiation (Fig. 6b), air temperature (Fig. 6d) and air humidity (Fig. 6e), which drive evaporation. With the upper bound influenced by PER, AER is dictated by VWC at the tailings surface, as it is mostly unsaturated during the monitoring period. The tailings temperature profile with depth (Fig. 7c) varied in similar trends to the air temperature, while the diurnal oscillation amplitude of tailings temperature decreased with depth. As the surface settlement might cause the top moisture sensors to be exposed to the air, the readings obtained from that topmost sensor were therefore removed from the graph after detachment from the column (e.g. the VWC at 15 mm below the surface was not shown after 14 May 2018 as the sensor was exposed to the air thereafter). The VWC of surface tailings was more sensitive to weather conditions than that of the underlying tailings. The moisture content near the surface may decrease from full-water saturation to completely dry by consecutive sun exposure and increase from air dry to full saturation due to rainfall, while the moisture content below the surface exhibited much fewer fluctuations (Fig. 7d). The bulk EC near the surface (Fig. 7e) was predominantly influenced by weather conditions, as it increased on rainy days and decreased during dry periods. Following a series of rainfall events in October 2018, the EC at 50 mm depth returned to zero as the sensor was exposed to the air. On the contrary, the bulk EC in the middle of the column ($\sim$ 600 mm below the initial column surface openings) appeared to be independent of weather conditions as it declined linearly at a slow rate before Mar 2019. However, when the top 150 mm of the column was removed in late Mar 2019, the EC in the middle of the column started to fluctuate following rainfall events as settlement caused the EC sensor to get closer to the tailings surface. The surface settlement and dry density increased after major rainfall events while barely changed in dry periods. At the end of the monitoring time, the tailings in the entire column were in high VWCs, similar to the tailings moisture profile observed at the beginning of the test, and settlement continued at a slow rate.

Based on the variations of VWC with depth (Fig. 7d) and the comparison between the potential evaporation and actual evaporation (Fig. 7b), the two-year monitoring time can be divided into five distinct periods, including four wetting–drying periods. In each wetting–drying period, the tailings started from a full-water-saturated condition, either as the initial tailings slurry or achieved by a series of rainfall events, and ended with the formation of a layer of unsaturated tailings that was achieved by a long period of desiccation. The fifth period represents a major wetting stage characterised by consecutive rainfall events and a relatively short drying time. The cumulative rainfall and evaporation in each period, along with VWC profiles with depth, is shown in Fig. 8. The images of the tailings surface at different stages of the test are displayed in Fig. 9.

The first wetting–drying period (period I) lasted for 27 days, starting from the beginning of the test to 7 May 2018, when 28 mm of rainfall occurred over two consecutive days, re-saturated the tailings in the column. The weather in the early stage of the first wetting–drying period was predominated by intermittent rainy and sunny days, which did not cause sufficient desiccation but led to about 15 mm of settlement (Fig. 8b). Subsequently, dry weather predominated for two weeks, leading to partial saturation of the top 130 mm of tailings (Fig. 8c). In the last week of this period, the unsaturated surface tailings caused a deviation of actual evaporation from potential evaporation (Fig. 7b), and this deviation increased as the tailings surface became drier. The cumulative actual evaporation was around 112 mm and increased linearly at an approximate rate of 5 mm/day in the first period, during which less than 48 mm of rainfall occurred (Fig. 8a). Such constantly high evaporation was attributed to the initial fully-saturated state of the freshly deposited tailings (identified from the colour of the surface tailings in Fig. 9a–d), which maintained a strong hydraulic connection between the surface and the underlying tailings. Only at the end of this period, the evaporation rate on the surface slowed down to less than 2 mm/day, with an unsaturated zone depth of 150 mm and a dry tailings layer of 15 mm near the surface (Fig. 8c).

The second wetting–drying period (period II) started on 8 May 2018 and lasted for 145 days until a series of intensive rainfall events occurred in October 2018, totalling 52 mm, which replenished the moisture storage within the tailings. 20 mm of settlement was achieved in a stepwise manner during this period (Fig. 8e). Similar to period I, the drying process started from a fully saturated condition. The depth of the unsaturated zone reached 80 mm below the surface in the first three weeks, after which evaporation almost ceased (Fig. 8d). The low surface evaporation rate allows the deeper tailings to gradually de-saturate (Fig. 8b). At the end of the drying period, de-saturation was identified to take place at 480 mm depth below the

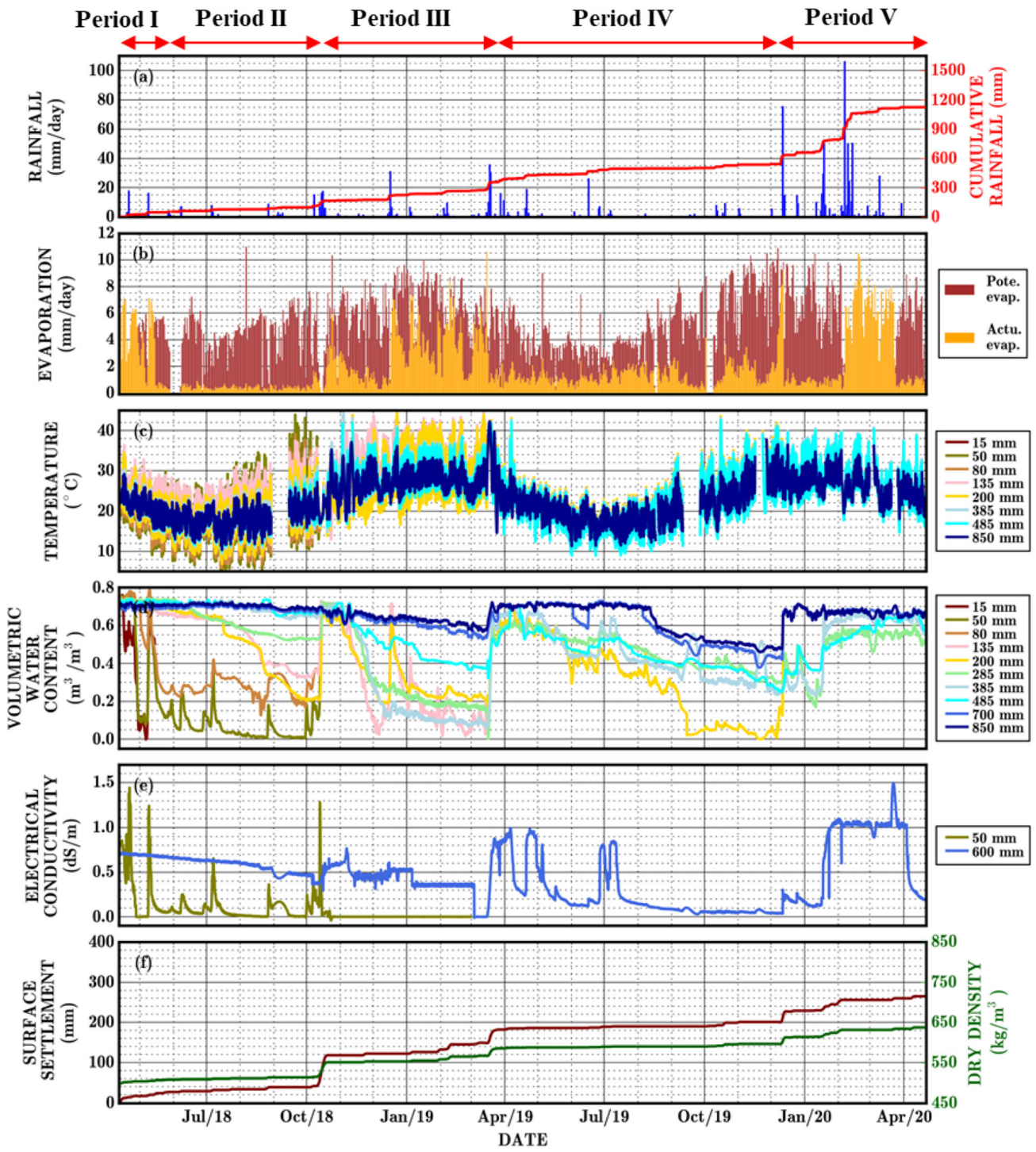


**Fig. 7** Monitored data over time, including **a** daily rainfall and cumulative data from the beginning of the test, **b** potential and actual evaporation derived from data of weather station using Penman-Monteith equation, **c** temperature and **d** volumetric water content of tailings at different depths, **e** electrical conductivity, and **f** surface settlement relative to the original elevation (1.2 m above the bottom of the column) and the corresponding dry density of tailings. The termination of the curves suggests the sensors are exposed to air due to surface settlement. The depth of the sensors as indicated in the legend is relative to the original column height, which is 1.2 m above the ground surface

surface, suggesting an unsaturated zone depth of ~ 500 mm. As a dry tailings layer was formed for the majority of this period, the cumulative actual evaporation (~ 100 mm) was much less than the cumulative potential evaporation (~ 600 mm), suggesting weather was not well utilised for tailings dewatering (Fig. 8d). Visual

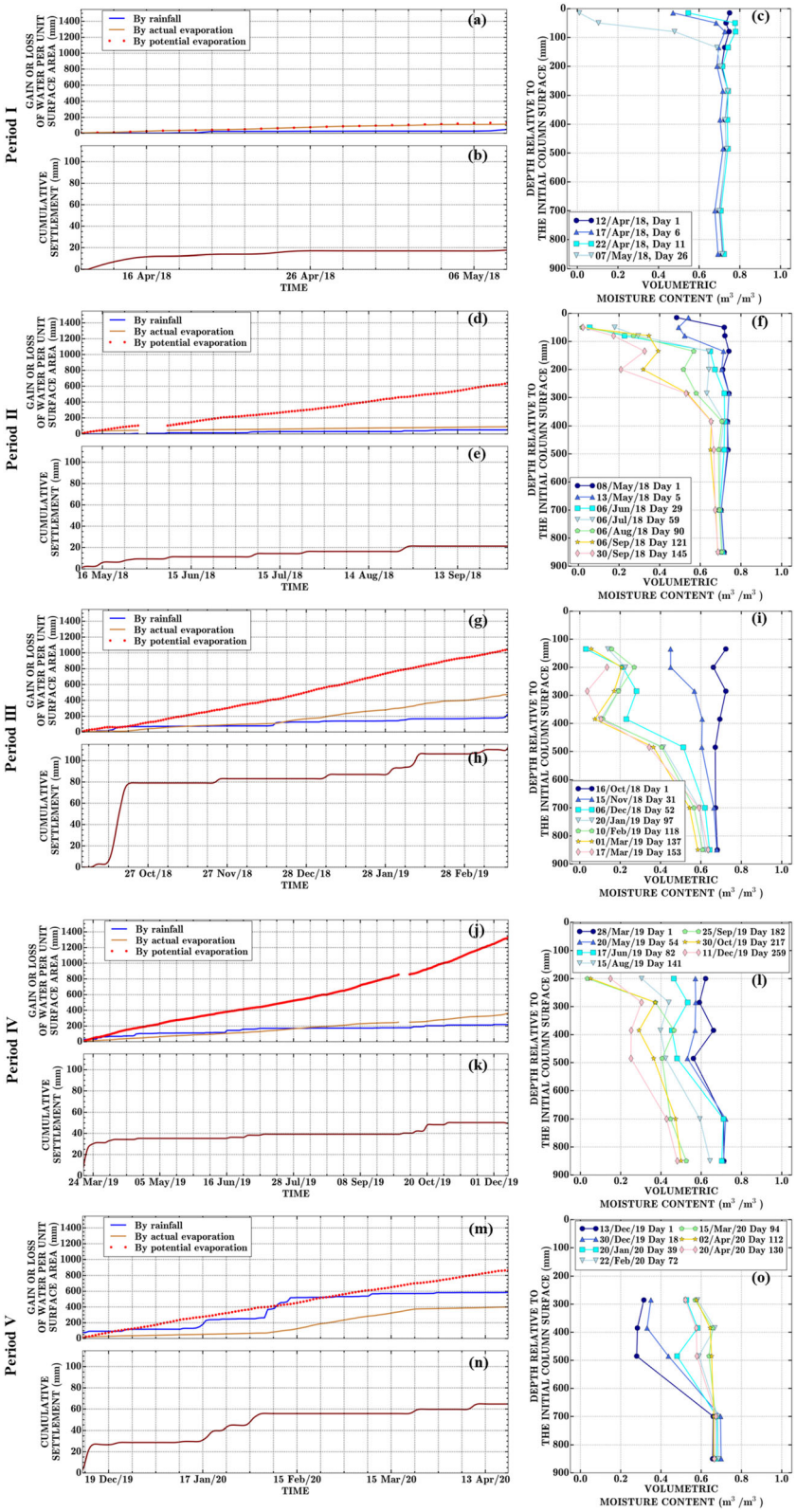


**Fig. 8** Evolutions of cumulative rainfall, actual evaporation, potential evaporation, settlement and monitored VWC profiles with depth in each period

observation identified that the colour of the surface tailings became lighter, consistent with the reduction of VWC (Fig. 9e–h). Besides, cracks developed on the surface tailings led to the formation of loose tailings layers, facilitating settlement after subsequent intense rainfall in the next period.

The third wetting–drying period (period III) began on 16 October 2018 after 12 days of heavy rainfall, over 80 mm in total, and lasted for 153 days until March 2019, when the top 150 mm section of the column was removed. The rainfall at the beginning of this period completely re-saturated the tailings. The rapid infiltration induced the collapse of an 80-mm-thick drying tailings skeleton near the surface and the formation of a pond above the surface (Fig. 9h and i), resulting in an increase of tailings dry density from 0.5 to 0.55 t/m$^3$ (Fig. 7f). In addition, the collapse led to the exposure of two moisture sensors (located at the depths of 50 mm and 80 mm). Following the rainfall, a completely dry tailings layer with a thickness of 300 mm was formed under high temperature and solar intensity for 100 days. The unsaturated zone developed to 700 mm depth, much thicker than that formed in period II (480 mm). The thickening of the unsaturated zone is attributed to the strengthened capillary forces during the two preceding wetting–drying periods, allowing for the transport of more water from deeper tailings to the surface for evaporation. The occasional rainfall that occurred during the 150 days of drying only moisturised the tailings near the surface, while tailings at deep layers seemed not to be affected by infiltration.

The fourth wetting–drying period (period IV), starting from 28 March 2019 and ending on 11 December 2019, lasted for about 259 days. Given 2019 was one of the driest years in the past 119 years [3], a maximum unsaturated depth could be naturally achieved during the desiccation. Only 40 mm of settlement was recorded during the first 200 days of this dry period, consistent with the previous observations that settlement barely occurred in dry periods. The moisture content measured by the bottommost moisture sensor (850 mm below the original tailings surface) reduced from 0.74 to 0.43, suggesting the depth of the unsaturated zone was more than 650 mm (given the cumulative settlement was 200 mm at that time), which represents the maximum depth achieved during the two-year monitoring period. Different from the previous three periods, where moisture content increased with depth prominently (Fig. 8c, f and i), in the fourth period, the moisture contents within the unsaturated zone were rather similar (Fig. 8l), suggesting the further enhancement of capillary forces due to increased dry density. During the drying process, salt started to precipitate on the tailings surface (Fig. 9n and o) and later vanished due to aeolian and diffusion processes (Fig. 9p). Instead of forming vertical cracks in the early periods, the surface of denser tailings tended to form scales during desiccation. Besides, precipitated salt and tailings crusting on the surface may impede further evaporation [9, 15, 34].

The fifth period (period V) encompassed a relatively long wet season (four months, from December 2019 to April 2020), during which moisture contents at different depths remained relatively high. After an intense rainfall of 78 mm on 12 December 2019 (Fig. 8m) (a maximum daily rate throughout the year 2019), an abrupt settlement of 23 mm occurred without any water ponded above the tailings surface. This is attributed to a large proportion of pore space in the unsaturated tailings formed during the preceding five months of the dry period with only 90 mm of rainfall. Such settling characteristics were also observed at the beginning of periods III and IV. In the subsequent three months, a series of rainfall events completely re-saturated the tailings and formed a 12-mm-deep pond above the surface (Fig. 9r and s). The actual evaporation rate was equal to the potential rate during the time when the pond existed (Fig. 8b), and the tailings below the pond experienced re-saturation and self-weight consolidation, resulting in an additional settlement of 38 mm. The weather became dry from late March 2020 to the end of period V (April 2020), lasting for 25 days, during which the unsaturated zone depth was about 415 mm and expected to be deeper if the test continued.

Although the first four periods can be regarded as repeated wetting–drying cycles, the tailings consolidated and desiccated in different manners. As the dry density of the tailings increased over time, the rainfall-induced surface settlement decreased gradually. For example, predominantly achieved by a single rainfall event, the settlement that occurred in the first year (from April 2018 to April 2019) was about 150 mm, almost the same as that (140 mm) during the second year (from April 2019 to April 2020), which was achieved through several rainfall events occurred in different seasons. Besides, surface cracks tended to form when the tailings had a relatively low bulk density (e.g. tailings in periods I and II), and the widths and depths of cracks increased with cumulative solar exposure. In contrast, salt precipitation and surface crusting were more common during the desiccation of mature tailings (e.g. tailings in periods IV and V). The maximum depth of the unsaturated zone from periods I to IV stretched downwards continually, mainly due to the strengthened capillary forces during tailings consolidation [36].

### 4.3 Characteristics of weather-induced consolidation and desiccation

Table 2 summarises the characteristics of tailings consolidation and desiccation behaviour at the end of the five

wetting–drying periods. Comparing the statistics at the end of the first four periods, both the overall thickness of the unsaturated tailings, the equivalent depth of the air phase (i.e. equivalent volume of water per unit surface to fill the air void in the tailings), and the effective volumetric air content in the unsaturated tailings (50%, 40%, 42% and 44%, respectively) increases monotonically. This is mainly due to the predominant desiccation that takes tailings water away and settlement that strengthens capillary forces in the unsaturated zone. Conversely, the thickness of the unsaturated tailings decreased greatly in the last period because the dry tailings layer had not yet formed at the end of period V, indicating that the unsaturated zone could be further developed as the test continued. Lasted for 27 days, Period I is featured by much higher average AER (4.15 mm/day) and higher cumulative normalised evaporation (the ratio of AER to PER [12]) (0.85) than the subsequent periods. Such high desiccation efficiency is attributed to the tailings experiencing the transition from slurry to solid state in this period, during which the surface remained predominantly wet. Different from period I, subsequent periods II, III and IV were much longer (145, 153 and 259 days, respectively), and tailings in these periods had formed into solid states, allowing the pore water in the sublayers to be desiccated. Although the time spans of periods II, III and V were similar (145, 153 and 130 days, respectively), the cumulative surface settlements attained in periods III and V (110 and 64 mm, respectively) were much more than that attained in period II (22 mm). Similarly, the cumulative normalised evaporations achieved in periods III and V the same (0.46), while over three times higher than that achieved in period II (0.14).

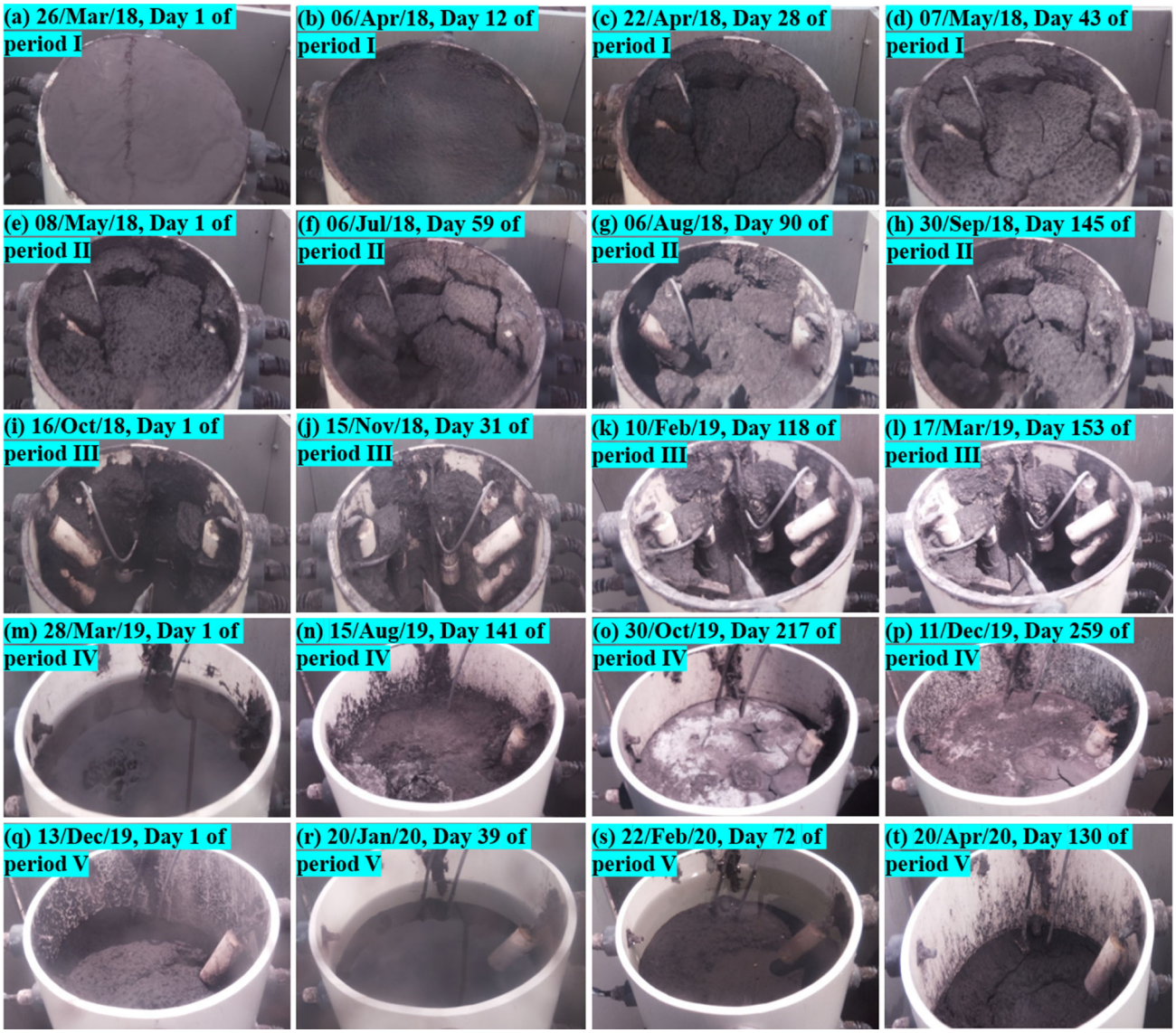


**Fig. 9** Images of the column surface at different stages of the test

**Table 2** Comparison of characteristics at the end of the five wetting–drying periods

| Wetting–drying period | I | II | III | IV | V |
|---|---|---|---|---|---|
| Time span (day) | 27 | 145 | 153 | 259 | 130 |
| Thickness of the unsaturated zone (mm) | 120 | 441 | 701 | 650 | 435 |
| Equivalent depth of the air phase in the unsaturated tailings (mm) | 60 | 176 | 292 | 286 | 58 |
| Cumulative rainfall (mm) | 47 | 51 | 226 | 219 | 584 |
| Cumulative potential evaporation (mm) | 132 | 633 | 1040 | 1329 | 866 |
| Cumulative actual evaporation (mm) | 112 | 91 | 474 | 366 | 399 |
| Cumulative normalised evaporation | 0.85 | 0.14 | 0.46 | 0.28 | 0.46 |
| Cumulative settlement (mm) | 17 | 22 | 110 | 52 | 64 |
| Average settlement rate (mm/day) | 0.63 | 0.15 | 0.72 | 0.20 | 0.49 |
| Average AER (mm/day) | 4.15 | 0.63 | 3.10 | 1.41 | 3.07 |
| Average PER (mm/day) | 4.89 | 4.37 | 6.80 | 5.13 | 6.66 |
| Effective volumetric air content in the unsaturated tailings (%) | 50 | 40 | 42 | 44 | 13 |
| Ratio of settlement to rainfall | 0.36 | 0.43 | 0.49 | 0.24 | 0.11 |
| Ratio of rainfall to AER | 0.42 | 0.56 | 0.48 | 0.60 | 1.46 |
| Porosity at the end of the period (−) | 0.74 | 0.74 | 0.71 | 0.69 | 0.67 |
| Dry density at the end of the period (kg/m$^3$) | 504.44 | 513.70 | 568.39 | 596.56 | 637.86 |

This is because periods III and V are in summer, with more rainfall (225 and 584 mm, respectively), higher solar exposure and stronger winds (with average potential evaporation rates of 6.80 and 6.66 mm/day, respectively) that facilitates both settlement and evaporation, whereas period II in winter that impedes these two processes. Despite rainfall promoting settlement by collapsing the cracks and cavities formed by desiccation, the ratio of the cumulative settlement to rainfall did not keep increasing but declined over time (0.37, 0.39, 0.49, 0.19 and 0.13, respectively), as the density of tailings increased through weather cycles. The average settlement rate in each period varied in a similar pattern to the average AER, suggesting that the tailings may settle fast when the surface desiccates at a relatively high rate. The ratio of cumulative rainfall to AER increased over time (from 0.42 in period I to 1.46 in period IV) and reached the highest in period V, indicating that the main source for surface evaporation after period I was from rainwater rather than the original tailings slurry. In period V, a pond was formed above the tailings surface due to frequent rainfall, resulting in re-saturation and self-weight consolidation of the tailings. As the surface settlement is visibly ongoing, the current monitoring test should continue to observe further variations in moisture profiles and volume changes.

Through the column test, tailings desiccation patterns could be evaluated through the evolution of surface evaporation and the unsaturated zone during weather cycles, and tailings consolidation could be characterised via the development of cumulative settlement and average settlement rate during weather cycles. It is noted that the tailings desiccation pattern in period III was different from other periods. Both the cumulative AER and the unsaturated thickness at the end of period III reached the maximum throughout the entire monitoring time. Despite having consolidated for half a year, the tailings still had relatively low dry density, and the surface layer was in a loose state (Fig. 9h). The weather during period III drove the desiccation of the early-consolidated tailings (low dry density without significant settlement) to the most extent, leading to rapid desiccation within the depth of 500 mm (average VWC was less than 0.2) and further de-saturation of tailings at lower layers. Loose tailings exhibited high desiccation efficiency in summer. With increasing proportions of air phases in the unsaturated zone, tailings tended to have significant settlement and even surface collapsed after normal rainfall events. In comparison, denser tailings had relatively low desiccation efficiency with the slow development of the unsaturated zone and settlement.

### 4.4 Water mass balance analysis

Figure 10 compares the water storage in the column derived externally from the water mass exchange between tailings and atmosphere (i.e. inflow from rainfall and outflow from actual evaporation) and that derived internally from moisture profile with depth and ponding water depth [17]. Overall, the changes in water mass obtained from the

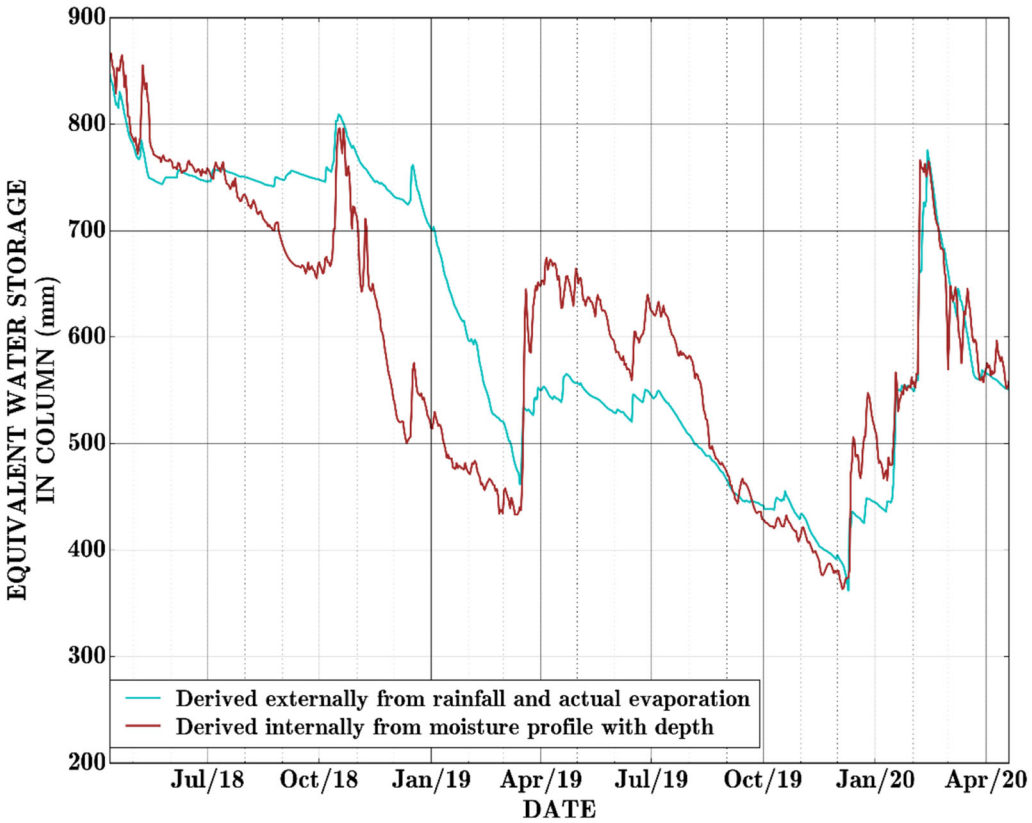


**Fig. 10** Water loss and gain in the tailings column over time estimated from the tailings-atmosphere exchange and moisture profiles with depth

two methods follow a similar pattern, particularly given that the water mass derived externally from the tailings-atmosphere exchange needs to integrate the recorded rainfall and evaporation at a 10-min interval over the 2-year monitoring period. Such agreement on the water balance obtained by the two methods also confirms the validity of Eq. (4) that extrapolates the degree of saturation on the surface using the saturation measurements from underlying moisture sensors, an important step to estimate actual evaporation using weather data, particularly in events of continuous settlement. However, the following discrepancies occurred between the two estimations:

1. When the surface tailings were wet (e.g. April 2018, March–August 2019 and December 2019–April 2020), the water mass derived from the moisture profiles tended to be more than that derived by the boundary exchange. This is probably because dewatering from tailings with high moisture content (generally greater than the plastic limit) might not trigger de-saturation, but rather consolidation or the reduction of ponding depth, which the moisture sensors were unable to identify.
2. During all major rainfall events identified by the rapid increase of water mass (e.g. May, November and December 2018, March, June and December 2019), the total water gain derived from the moisture profile appeared to be much higher than that obtained by the weather station, although the latter would, in general, be more accurate (as it is measured by calibrated tipping bucket). This may be induced by preferential infiltration into the tailings during rainfall events, which did not saturate the entire tailings layer but only the tailings around the sensors.
3. During the dry seasons between August 2018 and March 2019, the water mass that was derived from the moisture profile kept lower than that calculated from the mass exchange at the surface, with a maximum discrepancy of about 220 mm. Such deviation is likely caused by the development of cracks, which can be observed in Fig. 9. The downward propagation of cracks accelerates evaporation and hence loss of moisture content from deeper tailings. The acceleration could not be identified by the external method, where water loss was calculated by the AER from the surface that was much dryer than the underlying tailings. Despite offering distinctive water loss patterns, the two methods estimate almost the same cumulative water loss at the end of the drying processes. This is because the cracks only accelerate local drying, while affecting little the evaporative capillary strength and the depth of

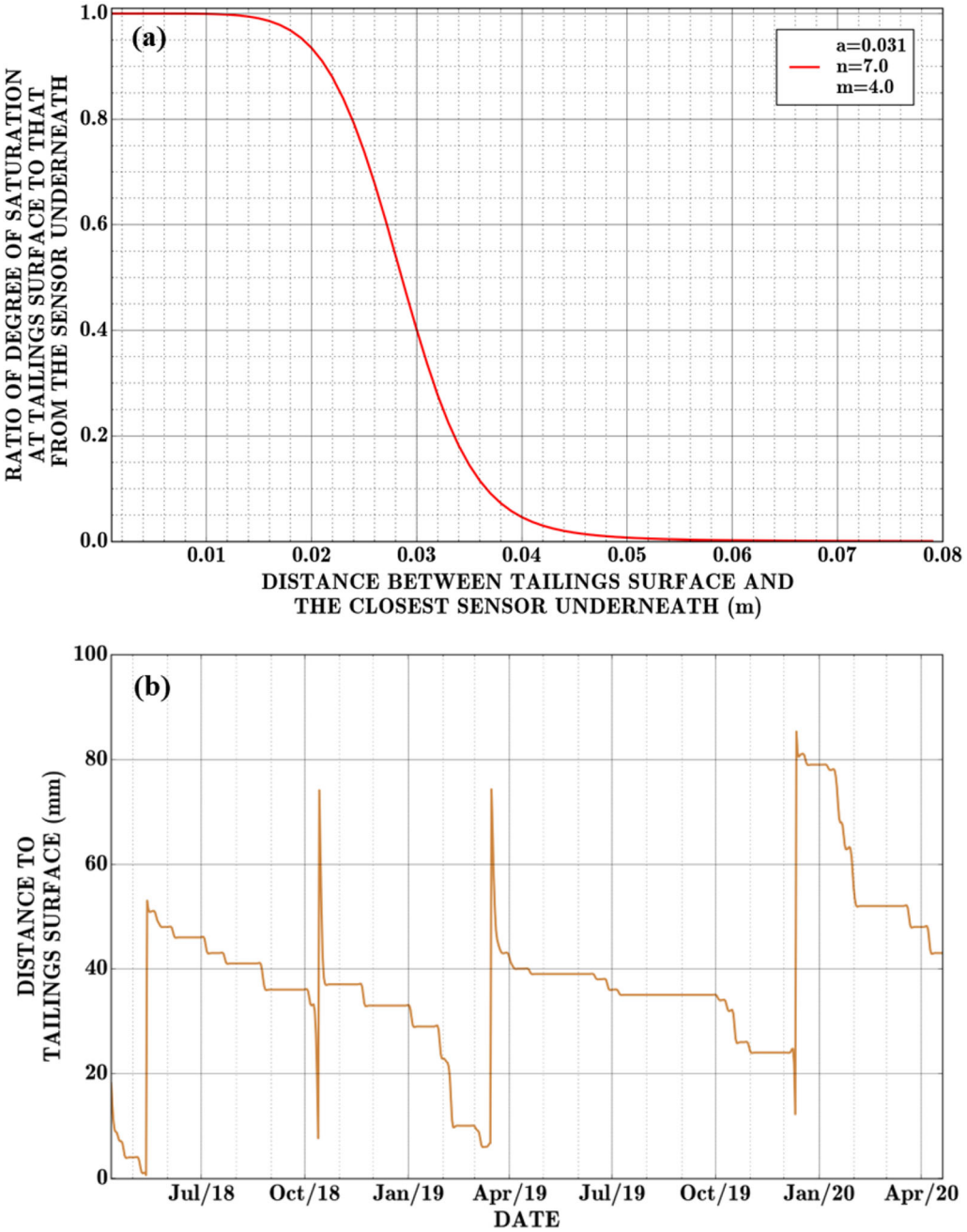


**Fig. 11** **a** Relationship between the ratio of $S_{rTS}$ to $S_r$ and their distance $D$; **b** distance between the tailings surface and the closest moisture sensor underneath

the unsaturated zone, which dictate the total amount of water loss by evaporation.

### 4.5 Discussion on the surface moisture extrapolation model

The evaluation of actual evaporation and the analysis of temporal water storage in the column through the mass exchange from the surface relies on the proposed Eq. (4) that extrapolates the moisture condition at the tailings surface ($S_{rTS}$), using the degree of saturation measured by an underlying moisture sensor ($S_r$) and its varying distance to the surface. Such a model is essential as the tailings surface keeps settling over time, while the elevations of the sensors are unchanged. A good agreement between the water mass derived from the tailings-atmosphere exchange and that from the moisture profile with depth, as shown in Fig. 10, can be achieved when parameters $a$, $n$ and $m$ in Eq. (4) are selected to be 0.031, 7 and 4.0, respectively.

Figure 11a shows the correlation between the ratio of the degree of saturation at the tailings surface and that at the closest underlying moisture sensor, and the depth from the surface to the moisture sensor ($D$). When $D$ is less than 20 mm, $S_{rTS}$ is almost the same as $S_r$. As $D$ increases from 20 to 50 mm, the ratio of $S_{rTS}$ to $S_r$ decreases rapidly, suggesting that the estimated moisture content surface may remain dry, regardless of that in the underlying tailings. Such estimation may describe the moisture profile in the unsaturated zone well during the drying processes, as the moisture content increases rapidly with depth. However, the assumption may not be valid during an episodic rainfall, where rainwater is only able to wet the tailings surface while insufficient to influence the moisture content of the underlying deep tailings where the sensor is located. Despite such inaccuracy, the persistent drying would eventually evaporate the limited rainwater retained at the surface, and so the assumption in the model is still valid over a long time scale, as indicated by the estimation of the water balance shown in Fig. 10. When $D$ is greater than 50 mm, $S_r$ is assumed to be zero, indicating the moisture data from the underlying sensor is no longer able to extrapolate the moisture condition at the tailings surface accurately. The selected parameters in the surface moisture extrapolation model and the maximum effective $D$ (a maximum distance between the tailings surface and the underlying moisture sensor to extrapolate the surface moisture and beyond that the ratio of $S_{rTS}$ to $S_r$ keeps zero) are particularly applied to the studied coal tailings with silt-like characteristics that exhibit a strong water-holding capacity, leading to a rapid increase in the moisture content of the underlying tailings within a depth of 50 mm even though the surface becomes dry, as shown in Fig. 8c and f.

Figure 11b shows the temporal variations of $D$. Throughout the two-year monitoring period, four major settlement events (where $D$ increases abruptly) occurred following heavy rainfall that caused significant increases in the water storage of the column (e.g. May and October 2018, March and December 2019), resulting in five moisture sensors were exposed to the air consecutively (two moisture sensors were exposed to the air during the settlement occurred in October 2018). Except for the last period when the maximum distance reached 85 mm, the distance between the tailings surface and the underneath moisture sensor varied mostly from 25 to 40 mm. This range confirms the validity of the assumption regarding the effective range of $D$ for the studied coal tailings. Based on this, the ratio of $S_{rTS}$ to $S_r$ that is determined through the selected parameters in the model also contributes to well estimating the actual evaporation at the tailings surface and consequently is validated by the water mass balance analysis using both external and internal methods. It is noted that the empirical model would not be applied when ponding water exists above the tailings surface as the actual evaporation is equal to the potential one in this situation. Therefore, from February to March 2020, although $D$ decreased from 80 to 50 mm and correspondingly the ratio of $S_{rTS}$ to $S_r$ kept zero, the equivalent water storage in the column calculated by the two methods still matched well.

Note that when applying the model to other tailings or soils, the parameters in Eq. (4) and the corresponding effective range of $D$ would differ from the current values. Given the proposed Eq. (4) has only been validated in this study with material-specific parameters, future work should focus on exploring the applicability of the model in other scenarios and the relationship between parameter selection and soil types. With more attempts in various soil or soil-like materials, the proposed equation could be further validated and enhanced.

## 5 Conclusions

The paper presents a comprehensive testing method that combines both experimental and theoretical approaches to gain a quantitative understanding of the long-term sedimentation, consolidation and desiccation behaviour of silt-like coal tailings under natural weather variations. Slurried coal tailings were deposited in the column for testing for over two years under a typical sub-tropical climate with hot and humid in summer, cool and mild dry in winter. It is found that: (*a*) the desiccation of the coal tailings by sun and wind is the most effective during the first month of exposure because the actual evaporation is close to the potential evaporation, suggesting a deposition cycle time for the coal tailings of one month and an optimal thickness of 150 mm at the monitoring area, under the given climate conditions and tailings characteristics; (*b*) the maximum unsaturated depths achieved by evaporation during the four wetting–drying periods are found to increase over time (120 mm, 441 mm, 701 mm and over 650 mm, respectively, from the periods in sequence), as continuing consolidation of the tailings after weathering has led to an increase in bulk density, resulting in stronger capillary forces to uptake water from the deeper tailings; (*c*) settlement predominantly occurs after rainfall events, where dry coal tailings with cracks and cavities formed during desiccation collapse; (*d*) freshly deposited tailings tend to crack vertically under sunbaking, leading to abrupt settlement after incident heavy rainfall, whereas under long-term sun exposure, mature denser tailings tend to form crusts and solid salt on the surface.

An empirical model is developed to extrapolate the moisture condition at the tailings surface based on the moisture content measured from the underlying sensor and its distance to the surface, a key step to estimate actual

evaporation from tailings subjected to settlement, based on weather conditions. The model was used to estimate the water storage in the column through rainfall and evaporation data over two years, which agrees well with that obtained from the moisture sensor array measurements.

The column test aims to present the self-weight consolidation and desiccation efficiency of coal tailings slurry. Besides, quantitative analysis of tailings desiccation provides a better understanding of to what extent the coal tailings at different consolidation stages de-saturates and re-saturates under the semi-arid weather condition. As the settlement is still ongoing, the test should continue to monitor the desiccation and settlement of mature tailings until no significant volume change occurs so that the time span to complete self-weight consolidation during wetting–drying cycles can be estimated. Future work can also focus on testing the applicability of the empirical model in other soft soils and exploring the possible relationship between SWCC and the surface moisture extrapolation model.

**Acknowledgements** This research is financially supported by Stanwell Corporation Limited, and the authors are grateful for the support of the China Scholarship Council (CSC). Also, This work is co-funded by an Australian Research Council Discovery Projects (DP180104156 and DP19010372).

**Funding** Open Access funding enabled and organized by CAUL and its Member Institutions.



**Data availability** All data generated or analysed in this study are available from the corresponding author on reasonable request.

## References

1. Ahmed SI, Siddiqua S (2014) A review on consolidation behavior of tailings. Int J Geotech Eng 8:102–111. https://doi.org/10.1179/1939787913Y.0000000012
2. Allen RG, Pereira LS, Raes D et al (1998) Crop evapotranspiration-guidelines for computing crip water requirements-FAO irrigation and drainage paper 56. FAO Rome 300(9):D05109
3. Australian Bureau of Meteorology (2019) Annual climate statement 2019. BOM, Australian Government. http://www.bom.gov.au/climate/current/annual/aus/2019/#:~:text=The%20national%20total%20rainfall%20for,the%20119%20years%20since%201900. Accessed 9 Jan 2020
4. Australian Government (2016) Tailings management: Leading practice sustainable development program for the mining industry. https://www.industry.gov.au/sites/default/files/2019-04/lpsdp-tailings-management-handbook-english.pdf
5. Been K, Sills GC (1981) Self-weight consolidation of soft soils: an experimental and theoretical study. Géotechnique 32:283–285. https://doi.org/10.1680/geot.1981.31.4.519
6. Bo MW, Choa V, Wong KS (2002) Compression tests on a slurry using a small-scale consolidometer. Can Geotech J 39:388–398. https://doi.org/10.1139/t01-112
7. Camillo PJ, RoJ G (1986) A resistance parameter for bare-soil evaporation models. Soil Sci 141:95–105. https://doi.org/10.1097/00010694-198602000-00001
8. Chakrabarti S, Horvath RG (1987) The theory of one-dimensional consolidation of saturated clays: part V, constant rate of deformation testing and analysis. Géotechnique 37:519–522. https://doi.org/10.1680/geot.1987.37.4.519
9. Chen XY (1992) Evaporation from a salt-encrusted sediment surface: field and laboratory studies. Aust J Soil Res 30:429–442. https://doi.org/10.1071/SR9920429
10. Daamen CC, Simmonds LP (1996) Measurement of evaporation from bare soil and its estimation using surface resistance. Water Resour Res 32:1393–1402. https://doi.org/10.1029/96WR00268
11. Daliri F, Simms P, Sivathayalan S (2016) Shear and dewatering behaviour of densified gold tailings in a laboratory simulation of multi-layer deposition. Can Geotech J 53:1246–1257. https://doi.org/10.1139/cgj-2014-0411
12. Entezari I, Rivard B, Lipsett MG, Wilson GW (2016) Prediction of water content and normalised evaporation from oil sands soft tailings surface using hyperspectral observations. Can Geotech J 53:1742–1750. https://doi.org/10.1139/cgj-2015-0416
13. Fečko P, Tora B, Tod M (2013) Coal waste: handling, pollution impacts and utilisation. The coal handbook: towards cleaner production. Woodhead Publishing, Cambridge, pp 63–84. https://doi.org/10.1533/9781782421177.1.63
14. Fredlund DG, Xing A (1994) Equations for the soil-water characteristic curve. Can Geotech J 31:521–532. https://doi.org/10.1139/t94-061
15. Fujimaki H, Shimano T, Inoue M, Nakane K (2006) Effect of a salt crust on evaporation from a bare saline soil. Vadose Zo J 5:1246. https://doi.org/10.2136/vzj2005.0144
16. Fujiyasu Y (1997) Evaporation behaviour of tailings. Dissertation, The University of Western Australia
17. Hemmati S, Gatmiri B, Cui YJ, Vincent M (2012) Thermo-hydro-mechanical modelling of soil settlements induced by soil-vegetation-atmosphere interactions. Eng Geol 139–140:1–16. https://doi.org/10.1016/j.enggeo.2012.04.003
18. Hoekstra P, Delaney A (1974) Dielectric properties of soils at UHF and microwave frequencies. J Geophys Res 79:1699–1708. https://doi.org/10.1029/jb079i011p01699
19. Indraratna B, Gasson I, Chowdhury RN (1994) Utilisation of compacted coal tailings as a structural fill. Can Geotech J 31:614–623. https://doi.org/10.1139/t94-074
20. Islam S, Williams DJ, Llano-Serna M, Zhang C (2020) Settling, consolidation and shear strength behaviour of coal tailings slurry. Int J Min Sci Technol 30:849–857. https://doi.org/10.1016/j.ijmst.2020.03.013
21. Jeeravipoolvarn S (2005) Compression behaviour of thixotropic oil sands tailings. Dissertation, University of Alberta
22. Lehmann P, Or D (2009) Evaporation and capillary coupling across vertical textural contrasts in porous media. Phys Rev E Stat Nonlinear Soft Matter Phys 80:1–13. https://doi.org/10.1103/PhysRevE.80.046318
23. Meng W, Sun X, Ma J et al (2019) Evaporation and soil surface resistance of the water storage pit irrigation trees in the Loess Plateau. Water 11:648. https://doi.org/10.3390/w11040648

24. Monteith JL (1981) Evaporation and surface temperature. Q J R Meteorol Soc 107:1–27. https://doi.org/10.1002/qj.49710745102
25. Olek BS, Pilecka E (2019) Large-scale Rowe cell experimental study on coefficient of consolidation of coal mine tailings. In: E3S Web of Conferences. pp 1–8. https://doi.org/10.1051/e3sconf/201910601004
26. Penman AD. (2001) Tailing Dams risk of dangerous occurrences. In: Geoenvironmental Engineering: Geoenvironmental Impact Management: Proceedings of the third conference organised by the British Geotechnical Association and Cardiff School of Engineering. pp 150–156
27. Penman HL (1948) Natural evaporation from open water, bare soil and grass. Proc R Soc London Ser A 193:120–145
28. Qiu Y, Sego DC (2001) Laboratory properties of mine tailings. Can Geotech J 38:183–190. https://doi.org/10.1139/cgj-38-1-183
29. Qiu Y, Sego DC (2007) Optimum deposition for sub-aerial tailings disposal: Model applications. Int J Mining Reclam Environ 21:65–74. https://doi.org/10.1080/17480930600906177
30. Rodríquez R, Sánchez M, Ledesma A, Lloret A (2007) Experimental and numerical analysis of desiccation of a mining waste. Can Geotech J 44:644–658. https://doi.org/10.1139/t07-016
31. Sample KM, Shackelford CD (2012) Apparatus for constant rate-of-strain consolidation of slurry mixed soils. Geotech Test J 35:409–419
32. Seneviratne NH, Fahey M, Newson TA, Fujiyasu Y (1996) Numerical modelling of consolidation and evaporation of slurried mine tailings. Int J Numer Anal Methods Geomech 20:647–671. https://doi.org/10.1002/(SICI)1096-9853(199609)20:9%3c647::AID-NAG844%3e3.0.CO;2-3
33. Shamsai A, Pak A, Bateni SM, Ayatollahi SAH (2007) Geotechnical characteristics of copper mine tailings: a case study. Geotech Geol Eng 25:591–602. https://doi.org/10.1007/s10706-007-9132-9
34. Shimojima E, Yoshioka R, Tamagawa I (1996) Salinisation owing to evaporation from bare-soil surfaces and its influences on the evaporation. J Hydrol 178:109–136. https://doi.org/10.1016/0022-1694(95)02826-9
35. Shokouhi A, Williams DJ, Kho AK (2014) Settlement and collapse behaviour of coal mine spoil and washery wastes. In: Proceedings of tailings and mine waste. Keystone, Colorado, pp 107–116
36. Shokouhi A, Zhang C, Williams DJ (2018) Settling, consolidation and desiccation behaviour of coal tailings slurry. Min Technol Trans Inst Min Metall. https://doi.org/10.1080/14749009.2017.1308691
37. Swarbrick GE, Fell R (1992) Modeling desiccating behavior of mine tailings. J Geotech Eng 118:540–557. https://doi.org/10.1061/(ASCE)0733-9410(1992)118:4(540)
38. Topp GC, Davis JL, Annan AP (1980) Electromagnetic determination of soil water content. Water Resour Res 16:574–582. https://doi.org/10.1029/WR016i003p00574
39. Van de Griend AA, Owe M (1994) Bare soil surface resistance to evaporation by vapor diffusion under semi-arid conditions. Water Resour Res 30:181–188. https://doi.org/10.1029/93WR02747
40. Vidler A, Buzzi O, Fityus S (2020) Effect of coal on mine tailings' water permeability and water retention. E3S Web Conf 195:03004. https://doi.org/10.1051/e3sconf/202019503004
41. Williams DJ (2012) Some mining applications of unsaturated soil mechanics. Geotech Eng 43:83–98
42. Wong RC, Mills BN, Liu YB (2008) Mechanistic model for one-dimensional consolidation behavior of nonsegregating oil sands tailings. J Geotech Geoenviron Eng 134:195–202. https://doi.org/10.1061/(asce)1090-0241(2008)134:2(195)
43. Zhang C (2014) Hydrodynamic and thermodynamic processes during evaporation from bare soils. Dissertation, The University of Queensland
44. Zhang C, Li L, Lockington D (2014) Numerical study of evaporation-induced salt accumulation and precipitation in bare saline soils: mechanism and feedback. Water Resour Res 50:8084–8106. https://doi.org/10.1002/2013WR015127
45. Zhang C, Li L, Lockington D (2015) A physically based surface resistance model for evaporation from bare soils. Water Resour Res 51:1084–1111. https://doi.org/10.1002/2014WR015490
46. Znidarčić D, Schiffman RL, Pane V, Croce P, Ko HY, Olsen HW (1986) The theory of one-dimensional consolidation of saturated clays: part V, constant rate of deformation testing and analysis. Géotechnique 36:227–237. https://doi.org/10.1680/geot.1986.36.2.227
47. Zreik DA, Germaine JT, Ladd CC (1997) Undrained strength of ultra-weak cohesive soils: relationship between water content and effective stress. Soils Found 37:117–128. https://doi.org/10.3208/sandf.37.3_117